Lasers in Manufacturing Conference 2023

Reinforcing cold working steel by high-speed laser melt injection

Philipp Warneke[a,*], Philipp Hildinger[a], Annika Bohlen[a], Thomas Seefeld[a, b]

[a]*BIAS – Bremer Institut für angewandte Strahltechnik, Klagenfurter Straße 5, 28359 Bremen, Germany*
[b]*MAPEX Center for Materials and Processes, Am Biologischen Garten 2, 28359 Bremen, Germany*

Abstract

High-speed laser melt injection (HSLMI) is a new method for generating extremely wear-resistant metal matrix composite (MMC) layers on tool surfaces with high productivity. In contrast to high-speed laser cladding, no additional matrix-forming material is needed. HSLMI can be applied on tools made of various materials whenever high demands are placed on both wear resistance and efficiency in terms of manufacturing time and costs. For injecting spherical fused tungsten carbide (SFTC) particles into the cold working steel 1.2362, process speeds of up to 100 m/min could be reached. Furthermore, this tool steel represents a challenging material due to its high susceptibility to cracking, and it was found that the formation of cracks inside the steel matrix can be reduced significantly by increasing the process speed.

Keywords: laser melt injection; metal matrix composite; wear protection

1. Introduction

Until now, the applications of laser melt injection (LMI) are strongly limited due to low process speeds and low productivity. Usually, the process speeds in LMI are below 2 m/min (Student et al., 2018). In contrast, process speeds between 5 m/min (Sommer et al., 2021) and 400 m/min (Wank et al., 2022) are possible in laser cladding. In LMI, hard particles without any matrix-forming material are transported by a feeding gas towards the weld pool, see Figure 1. Usually, feeding gas volume flow rates below 5 l/min are used (Jendrzejewski et al., 2009). Recently, it was shown that the particle velocity, which can be adjusted via

* Corresponding author. Tel.: +49-421-218-58041; fax: +49-421-218-58063.
E-mail address: warneke@bias.de.

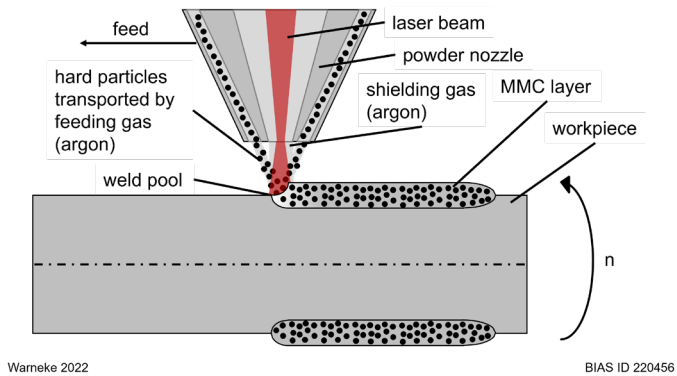

Fig. 1. Schematic illustration of laser melt injection

the feeding gas volume flow rate, is a key factor for enabling high process speeds (Warneke et al., 2023). By applying a particle velocity of 9 m/s, process speeds of up to 100 m/s could be reached.

As hard materials for reinforcing metallic surfaces by LMI, metallic hard materials are used in particular. These are carbides, borides and nitrides of transition metals of the IVa-, Va- und VIa-group in the periodic table (Schatt et al., 2007). Due to a poor wetting behavior, nitrides are less important for LMI (Schedler, 1988; Arth et al., 2014). Among the carbides, spherical fused tungsten carbide (SFTC) is a very suitable hard material for LMI due to a high hardness of up to 3100 HV0.1 and a good wetting behavior (Oerlikon Metco, 2016). However, it is well known that fused tungsten carbide particles partially degrade in welding-related processes. A degradation seam around the particles is formed in nickel (Vespa et al., 2012) and cobalt (Zanzarin et al., 2015) based matrices. Furthermore, in LMI, the SFTC particles can partially melt and lose their spherical shape due to interactions with the laser beam. In lubricant-free deep drawing, a precise melting of SFTC particles can be used to generate fused tungsten carbide nuggets that reduce the contact pressure (Ditsche and Seefeld, 2020).

2. Experimental Methods

2.1. Materials

The substrate was made of 1.2362 (X63CrMoV5-1) which is a cold work steel typically used for rolls. SFTC particles (Oerlikon MetcoClad 52001) featuring a grain fraction between 45 µm and 106 µm were injected into the 1.2362 substrate by LMI. SFTC is an eutectic material of 20 … 27 % WC and 73 … 80 % W2C (Nowotny et al., 2014).

2.2. High-speed laser melt injection

The laser beam of a disc laser (Trumpf TruDisk 12002) with a wavelength of 1030 nm was guided to a processing optic (Trumpf BEO D70) by an optical fiber with a diameter of 200 µm. The collimating lens of the processing optic provided a focal length of 200 mm, whereas the focusing lens provided a focal length of 300 mm. The processing optic was carried by a six-axis robot (Reis) that moved the processing optic parallel to the rotational axis of the workpiece. The workpiece was positioned 15 mm below the laser focus obtaining a laser spot with a diameter of 2 mm. A three-jet powder nozzle (IXUN) with a working distance of 16 mm was used. The SFTC particles were transported to the powder nozzle by a powder feeder (GTV PF 2/2). Argon was used as feeding gas and as shielding gas. The overlapping degree was set to 50 %.

2.3. Metallographic analysis

The MMC specimens were cut by an EDM machine (Mitsubishi MV 1200 V) and hot mounted into Struers LevoFast. After grinding the mounted specimens with a granulation from P320 to P1000, they were polished by a diamond suspension featuring a particle size of 3 µm and by a silica suspension featuring a particle size of 0.04 µm. For investigating the microstructure of the MMC layers, the samples were etched by Beraha I. Micrographs were taken with a light microscope (Zeiss AX10). The software ImageJ was used for measuring the cumulated crack length, the porosity and the width of the degradation seam. For measuring the porosity, a ROI with an area of 1.8 mm² was analyzed for MMC layers with a layer thickness up to 400 µm and two ROI with an overall area of 3.6 mm² were analyzed when the MMC layer thickness exceeded 400 µm. The cumulated crack length was defined as the sum of all crack lengths in a ROI of 2 mm² within the MMC layer. Only cracks within the 1.2362 matrix were considered. Furthermore, a hardness tester (Struers DuraScan 50) was used for measuring the Vickers hardness HV 0.1. For analyzing the SFTC degradation, an SEM (Zeiss EVO) and an EDX detector (Bruker Quantax) were used.

3. Results and Discussion

The particle velocity can be adjusted via the volume flow rate of the feeding gas. The correlation is shown in Figure 2. It was found that the particle velocity needs to be increased to 9 m/s for avoiding undesired deformations of SFTC particles, see Figure 3. For this, the volume flow rate needs to be increased from 5 l/min to 15 l/min. By increasing the particle velocity, both the travel time between powder nozzle and weld pool and the incorporation time of the particles can be reduced. Consequently, interactions with the laser beam are reduced as well and the initial geometry of the SFTC particles is preserved. Negative effects due to the increased volume flow rate of the feedings gas were not observed.

With a particle velocity of 9 m/s, the process speed of LMI could be increased up to 70 m/min with a laser power of 6.7 kW and up to 100 m/min with a laser power of 10 kW. A process speed of 100 m/min

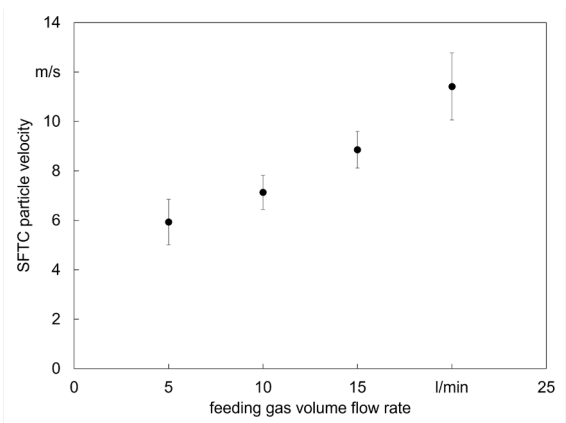

Fig. 2. Correlation between the volume flow rate of the feeding gas and the average velocity of the SFTC particles

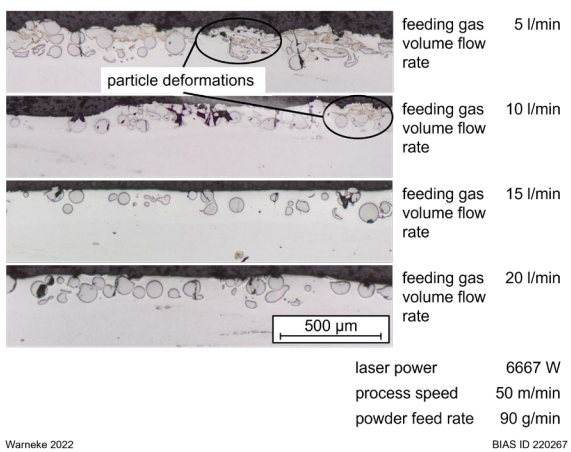

Fig. 3. Cross sections of SFTC particle reinforced 1.2362 obtained by HSLMI with different volume flow rates of the feeding gas

corresponds to a processed area per unit time of 1000 cm²/min under the given process parameters. With HSLMI, near-net shape MMC layers featuring a small layer thickness can be generated, see Figure 4. The interface between the SFTC particles and the 1.2362 matrix shows a good metallurgical bonding. Only a few particle deformations were detected. Furthermore, cracks within the 1.2362 matrix were detected that also run through SFTC particles. The cracks are mainly oriented perpendicular to the surface.

Cracks and pores were detected at all investigated process speeds. Both the porosity and the cumulated crack length decrease degressively with increasing process speed, see Figure 5. The porosity can be reduced from 6 vol% to 1 vol% and the cumulated crack length from 6 mm to 1 mm by increasing the process speed from 10 m/min to 70 m/min. At a process speed of 10 m/min, the porosity and the cumulated crack length are significantly higher than at higher process speeds. It can be concluded that high process speeds lead to a reduction of the heat input due to a low energy per unit length and accordingly to a reduction of temperature-related defects.

Furthermore, the process speed has a major influence on the microstructure of the MMC layer. A heterogenous microstructure consisting of martensite regions (etched blue to brown) and retained austenite regions (white) was found at all investigated process speeds between 10 m/min and 70 m/min. The austenite regions feature a fine dendritic structure as shown in Figure 6. Between a process speed of 10 m/min and 50 m/min, the martensite grains feature a rounded shape, see Figure 6. The SFTC particles are strongly degraded. When the process speed is further increased to 60 m/min and 70 m/min the microstructure of the martensite regions changes to a needle-shaped structure, see Figure 7. The degradation seam of the SFTC particles is significantly smaller than at lower process speeds. A drop in hardness can be found both for the white regions and for the brown/ blue regions of the 1.2362 matrix when increasing the process speed from 10 m/min to 70 m/min, see Figure 8. The average hardness of the white regions decreases from 907 HV 0.1 to 612 HV 0.1 whereas the average hardness of the brown/ blue regions decreases from 1078 HV 0.1 to 795 HV 0.1. In contrast, the SFTC particles did show no significant drop in hardness. However, the hardness drops from 2853 HV 0.1 in the SFTC particles to 973 HV 0.1 in the SFTC degradation seam at a process speed of 10 m/min. No hardness could be measured for the SFTC degradation seam at a process speed of 70 m/min because the degradation seam width is too small.

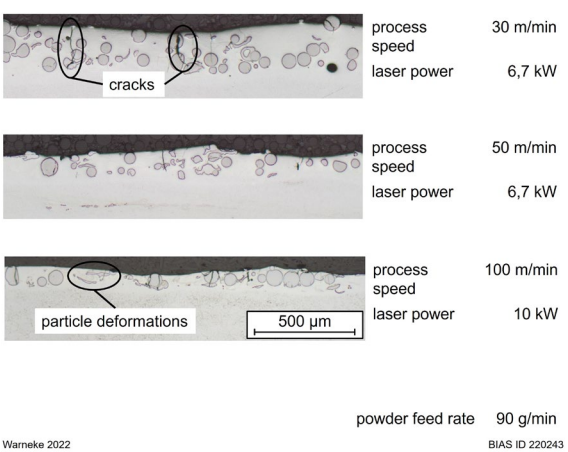

Fig. 4. Cross sections of SFTC particle reinforced 1.2362 obtained by HSLMI

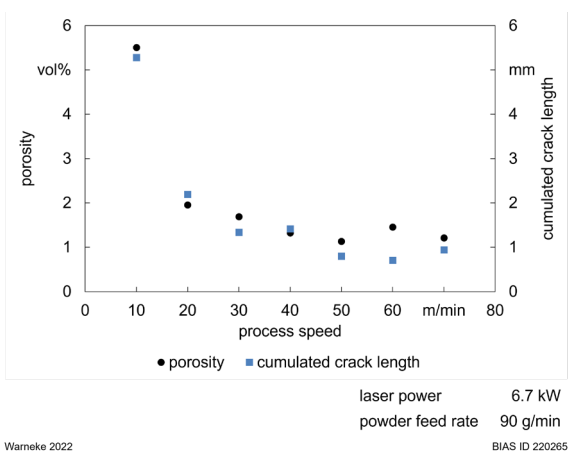

Fig. 5. Porosity and cumulated crack length as a function of the process speed

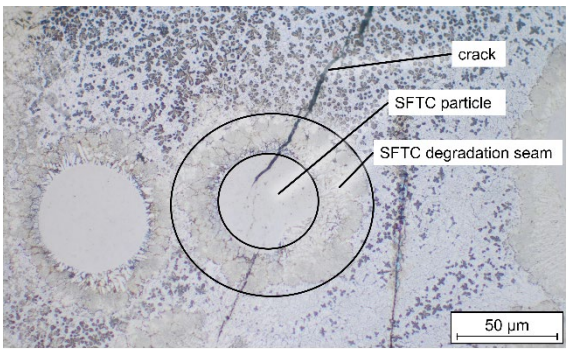

Fig. 6. Microstructure of SFTC particle reinforced 1.2362 obtained by HSLMI at a process speed of 10 m/min. Flat section etched by Beraha I

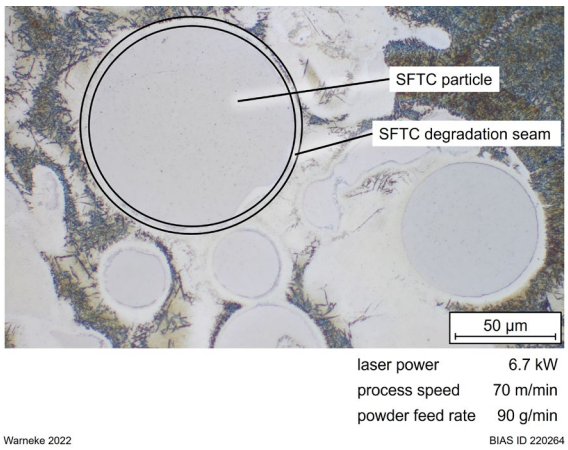

Fig. 7. Microstructure of SFTC particle reinforced 1.2362 obtained by HSLMI at a process speed of 70 m/min. Flat section etched by Beraha I

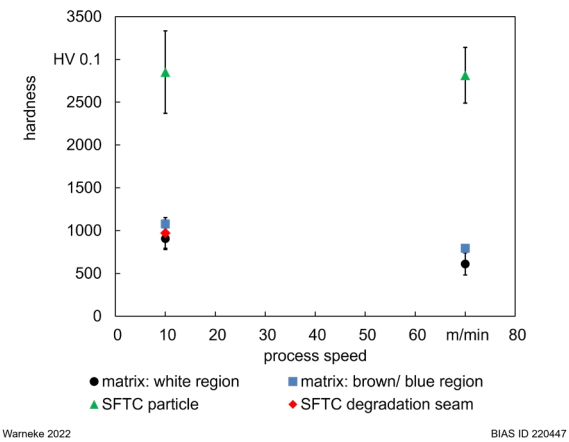

Fig. 8. Micro hardness of 1.2362 matrix, SFTC particles and SFTC degradation seam

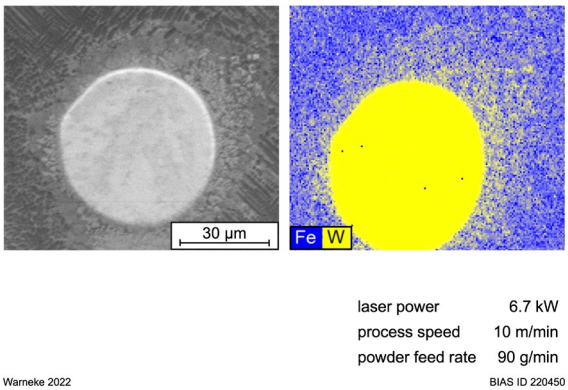

Fig. 9. SEM image (left) and EDX mapping (right) of an SFTC particle featuring a degradation seam within a 1.2362 matrix

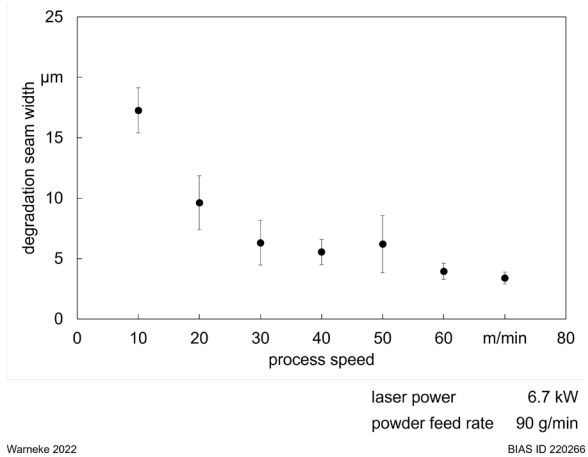

Fig. 10. Degradation seam width of SFTC particles as a function of the process speed

The SFTC degradation at a process speed of 10 m/min was analyzed by EDX. Figure 9 (right) shows that the degradation seam is rich in tungsten and iron meaning that parts of the SFTC particles dissolve in the surrounding 1.2362 matrix. The average tungsten content within the SFTC degradation seam is 36.8 wt%. The dependency of the SFTC degradation from the process speed was investigated from 10 m/min to 70 m/min. Figure 10 shows that the width of the degradation seam decreases degressively with increasing process speed. By increasing the process speed from 10 m/min to 70 m/min the width of the SFTC degradation seam can be reduced from 17 µm to only 3 µm.

At high process speeds, the lifetime of the melt pool is significantly smaller which reduces the time for SFTC degradation. The degradation process is based on diffusion which is time- and temperature-dependent (Günther et al., 2018). In order to preserve the desired material properties, the SFTC degradation should be minimized, especially since there is a significant drop in hardness in the degradation seam.

4. Conclusions

It was found that the particle velocity is a key factor for enabling LMI at high process speeds. With HSLMI, process speeds of up to 100 m/min can be reached. The process speed has a major influence on the MMC microstructure. The cumulated crack length and the porosity within the 1.2362 matrix decrease strongly when increasing the process speed. The SFTC particles show a degradation seam. The SFTC degradation can be reduced by increasing the process speed.

Acknowledgements

The authors gratefully acknowledge the support of this work by Deutsche Forschungsgemeinschaft (DFG) within the projects 424737129 and 495532447.

References

Arth, G., Bernhard, C., Samoilov, A. & Samek, L., 2014. Entwicklung von Stahl-Keramik-Verbunden mit verminderter Dichte, BHM Berg- und Hüttenmännische Monatshefte 159, 291–293.

Ditsche, A. & Seefeld, T., 2020. Local Laser Particle Fusion: Fusing of Hard Particles for the Reduction of High Contact Pressures in MMC Tool Surfaces, JOM 72, 2488–2496

Günther, K., Liefeith, J., Henckell, P., Ali, Y. & Bergmann, J.P., 2018. Influence of processing conditions on the degradation kinetics of fused tungsten carbides in hardfacing, International Journal of Refractory Metals and Hard Materials 70, 224–231.

Jendrzejewski, R., van Acker, K., Vanhoyweghen, D. & Śliwiński, G., 2009. Metal matrix composite production by means of laser dispersing of SiC and WC powder in Al alloy, Applied Surface Science 255, 5584–5587.

Nowotny, S., Berger, L.-M. & Spatzier, J., 2014. Coatings by Laser Cladding, in Comprehensive Hard Materials 1, Sarin, V.K., Mari, D. & Llanes, L., 507–525.

Oerlikon Metco, 2016. Material Product Data Sheet - Spherical Cast Tungsten Carbide Powder for Laser Cladding, https://www.oerlikon.com/metco/en/products-services/coating-materials/laser-pta-weld-overlay/laser-cladding/, accessed on 08/13/2020.

Schatt, W., Wieters, K.-P. & Kieback, B., 2007. Pulvermetallurgie, Springer-Verlag.

Schedler, W., 1988. Hartmetall für den Praktiker, VDI-Verlag GmbH.

Sommer, N., Stredak, F. & Böhm, S., 2021. High-Speed Laser Cladding on Thin-Sheet-Substrates—Influence of Process Parameters on Clad Geometry and Dilution, Coatings 11, 1–21.

Student, M., Pokhmurska, H., Zadorozhna, K., Dzyubyk, A. & Khomych, I., 2018. Structure and wear resistance of aluminium alloys coated with surface layer laser-modified by silicon carbide, Ukrainian Journal of Mechanical Engineering and Materials Science 4, 49–57.

Vespa, P., Pinard, P.T., Gauvin, R. & Brochu, M., 2012. Analysis of WC/Ni-Based Coatings Deposited by Controlled Short-Circuit MIG Welding, Journal of Materials Engineering and Performance 21, 865–876.

Wank, A., Schmengler, C., Krause, A., Müller-Roden, K. & Wessler, T., 2022. Environmentally Friendly Protective Coatings for Brake Disks, Journal of Thermal Spray Technology.

Warneke, P., Bohlen, A. & Seefeld, T., 2023. Influence of the process speed in laser melt injection for reinforcing skin-pass rolls, Journal of Laser Applications 35.

Zanzarin, S., Bengtsson, S. & Molinari, A., 2015. Study of carbide dissolution into the matrix during laser cladding of carbon steel plate with tungsten carbides-stellite powders, Journal of Laser Applications 27.